INFRARED SCATTERING BY SILICON CRYSTALS

DAVID F. WAGNER

INFRARED SCATTERING

BY SILICON CRYSTALS

* * * * *

David F. Wagner

INFRARED SCATTERING

BY SILICON CRYSTALS

by

David F. Wagner

Lieutenant, United States Navy

Submitted in partial fulfillment of
the requirements for the degree of

MASTER OF SCIENCE

United States Naval Postgraduate School
Monterey, California

1 9 6 2

INFRARED SCATTERING BY SILICON CRYSTALS

BY

David F. Wagner

This work is accepted as fulfilling
the thesis requirements for the degree of

MASTER OF SCIENCE

from the

United States Naval Postgraduate School

ABSTRACT

Incoherent infrared scattering of silicon is reviewed and scattering from a crystal grown along a <110> axis has been examined. It is concluded that the incoherent infrared scattering arises from regions in the cyrstal bounded by dislocation loops. The observed radii of cyration of the scattering regions, $\simeq 5\mu$, agree with the size of dislocation loops which are observed using Dash's decorating technique. Analysis of the small angle scattering precludes the presence of oxide particles smaller than about 1μ, and microscopic examination discloses no particles larger than this indicating that there has been no coalesence of oxides.

TABLE OF CONTENTS

LIST OF ILLUSTRATIONS

CHAPTER I

INTRODUCTION

Infrared radiation has been employed by many investigators in attempts to study imperfections in the structure of silicon crystals. The majority of efforts have been directed toward the deliniation of dislocation and impurity defects. Chemical etching has long been used as a means of visual detection of the emergence of dislocations at crystal surfaces. A method of creating images of dislocations within the bulk of the crystal by a decorating technique has been developed by Dash[1,2] at the General Electric Laboratories. He was able to trace visually the dislocation lines through the crystal and detect their emergence at etch pits at the surface. X-ray extinction microscopy has been applied in determining dislocation densities.[3,4] A unique method using an integrating sphere to detect light scattering by both dislocations and oxide impurities was used at the General Telephone and Electronics Laboratories.[4]

This investigation was directed toward the application of incoherent scattering techniques as a means of particle size determination in silicon crystals. Small angle X-ray diffraction is a well established method used to measure particle sizes of the order of magnitude of X-ray wavelength. However, this method is not applicable to structure determinations of sizes large compared to the wavelength of the radiation used. Theoretically, with longer wavelengths, one could determine the sizes of larger particles. The problem encountered is that softer X-rays and visible light are attenuated to quickly by matter. The wavelengths in the

near infrared spectrum are of the magnitude of dislocation and impurity networks observed by the methods referred to above. Therefore, incoherent scattering of infrared appears to offer possibilities as another means of determining the dislocation densities within silicon crystals. It is also proposed that a diffraction system can be built easily and cheaply thus avoiding the highly designed and costly equipment associated with X-ray diffraction and small angle cameras.

CHAPTER II

REVIEW OF DISLOCATION AND OXIDE IMPURITY DETECTION IN SILICON CRYSTALS

1. Chemical Etching - A method of identifying dislocations in LiF crystals by observations of etch-pits reported by Gilman[5] has been applied to semi-conductor materials by other investigators (Vogel et al[6], Dash[7,8]). Dash's work was devoted to the study of dislocations in silicon crystals. He reported etch-pits several hundred microns in diameter extending a comparable distance into the crystal when etched overnight with an echant consisting of the following parts by volume: 1 50% HF, 3 70% HNO_3, 10 glacial acetic acid. One can obtain the dislocation density of a crystal by counting the etch-pits which mark the emergence of dislocations at the crystal surface. Dash observed deep pits on any surface independent of its crystallographic direction. The dislocation density within any one crystal may vary strongly with orientation, and etch-pit counts on only one surface can lead to erroneous conclusions about crystal perfection. Schwuttke[4] reported errors up to 100 per cent in crystals of low dislocation density. Etch-pit counting is universally applied by investigators as a means of obtaining dislocation densities in silicon crystals.

2. Decoration - Dash[7,8] describes a technique for observing visually the dislocation lineage within the bulk of silicon crystals. Copper atoms diffused into the crystal were precipitated in aggregates along dislocations after appropriate heat treatment. Silicon but not copper, is transparent to near infrared radiation. Using an infrared image tube

fitted with a microscope he was able to obtain images of dislocation lineages in the crystals. A one to one correlation between the images and dislocations was obtained by tracing the lines to etch-pits at crystal surfaces. Precipitates are frequently not found on pure screw dislocations, but when formed they appear as tightly wound helicies. In $\langle 110 \rangle$ grown crystals he observed dislocation loops ranging up to 50 microns in diameter. Copper atoms appear as a fine, speckeled substructure in dislocation-free crystals. This is apparently a result of agglomeration of the precipatate throughout the crystal body.

3. Light Scattering

a. Integrating Sphere Technique - Schwuttke[4] reports a method of detecting incoherent scattering of infrared by "bad regions" within silicon crystals. He calculated the number of scattering centers (regions outlined by dislocations) necessary to produce detectible scattering. Three assumptions were made: 1. Imperfection scattering, to be observable, must be ten times greater than thermal scattering, 2. The scattering centers are spherical in shape, 3. The radius of the scattering centers is of the order of 0.1 micron. Since the particle size is small comparted to the wavelength of the radiation ($\lambda = 1.1\mu$), expressions for Rayleigh scattering are developed relating intensity to the size and number of bad regions per unit volume. Theoretical considerations suggest that a dislocation density of at least 10^8 per cm^2 is necessary to produce observable scattering. This was confirmed in Schwuttke's experiment, but the results do not constitute a confirmation of the assumed particle size. The object of the study was to determine the dislocation density necessary to produce scattering.

As previously noted, Dash reported dislocation loops of from 2-50 microns in diameter. Also the loops tend to lie in favorably orientated planes thus suggesting a platelet configuration. Regions of 0.1 micron (the assumed particle size in this study) described by dislocations cannot be resolved by Dash's method, but since the scattering depends on a radius of gyration there exists an infinite number of particle size and shape combinations which could produce the same scattering effect. Lacking supplementary information, one cannot draw definite conclusions about either size or shape.

Schwuttke's ingenious experimental technique of observing very small intensities of scattered radiation warrants a brief description. The optical arrangement of the instrument appears in figure 2-1.

A gold-plated integrating sphere contains a tungsten filiment light source S. The black body B and openings O_1 and O_2 define a conical umbra into which no light originating inside the sphere can penetrate. However, scattering by a crystal placed outside of O_2 will permit light to enter the "dark" area. With a suitable optical system and infrared image tube, scattered light can be observed.

b. X-ray Extinction - X-ray diffraction techniques have been used to substantiate dislocation counts in crystals obtained by the previously described techniques. The double-crystal spectrometer rocking curve method is commonly applied to determine crystal perfection. Lang[9] reports this method to be unreliable for dislocation densities below about 10^6 per cm^3. X-ray topographs can present an unambiguous display of dislocation lineage within a crystal. He was able to observe directly individual dislocations by copper atom decoration. Lang's results substantiate the preference of the $\langle 110 \rangle$ direction for straight line

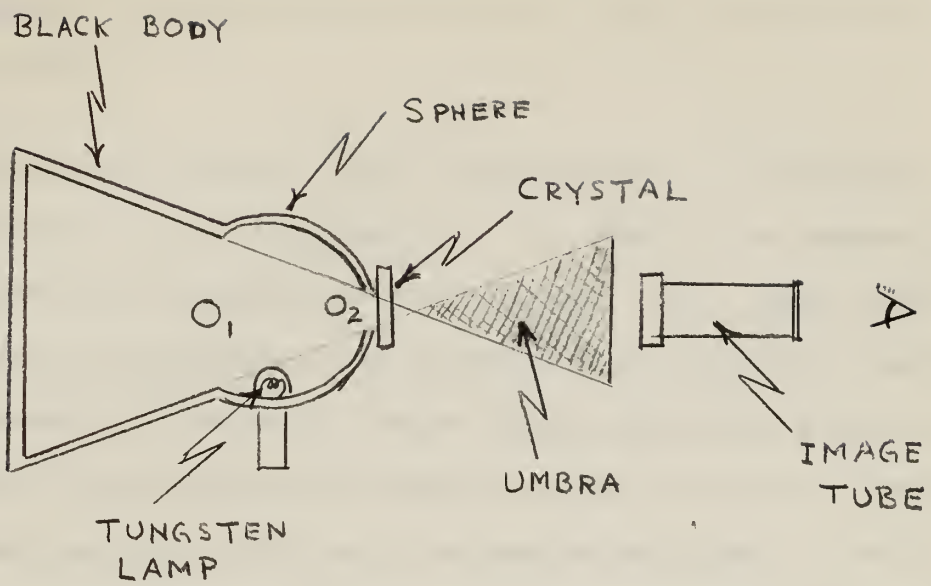

Fig. 2-1 Schwuttke's Scattering Integrating Sphere

dislocations reported by Dash. Arrays of hexagonal loops are formed by the closing of $\langle 110 \rangle$ edge dislocation lines by pure screw components. This suggests a thin two dimensional platelet type of configuration for a particle shape.

c. Additional Results - One incomplete report of dislocation observation was found in the literature. The results, but apparently not the experimental procedures, were published. Patel, Wagner and Moss[10] have observed the aggregation and collapsing of supersaturated vacancies to form condensed prismatic dislocation loops upon cooling silicon crystals from the melt. They report that indirect evidence of this was obtained by Chandhuri and Patel from plastic deformation experiments. The dislocation loops observed after deformation were estimated to be about 1 micron in diameter.

4. Oxygen Impurities - Oxygen impurities have been observed by both decoration and light scattering techniques. Several investigators have reported the effect of oxygen in contributing to erroneous dislocation etch-pit counts but have not used echants as a means of oxide detection.

Debye and Lederhandler[11] in an incomplete report state they have obtained SiO_2 particle sizes by measuring angular dependence of scattered infrared radiation. They found particle sizes of the order of the wavelength of the light. The sizes are strongly dependent upon the heat treatment given the specimens. Kaiser[12] reports the effect of long (50 hours) heat treatment at 1000°C on the optical properties of silicon. Prior to heating, silicon exhibits a sharp infrared absorption band at a wavelength of 9 microns. The absorption is proportional to oxygen concentration. Following heat treatment, the band decreases but without an

accompanying lowering in oxygen concentration. He attributes this to the clustering of silicon oxide into particles of lower dielectric constant than the silicon matrix.

Kaiser also makes an attempt at SiO_2 particle size determination by observation of Rayleigh scattering. He assumes a spherical particle of size smaller than the wavelength of radiation employed. Since Si and SiO_2 do not absorb at wavelengths of 1-3μ , changes in intensity will be due to Rayleigh scattering and not absorption. For spherical particles, the absorption coefficient (α) due to Rayleigh scattering is

$$\alpha = K N_p V^2 / \lambda^4 \qquad 2\text{-}1$$

where K is a constant, Np the number of scattering centers, V the total volume of scattering centers and λ the wavelength. Following the inverse 4th power law, a log-log plot of α vs. λ should yield a straight line of slope equal to -4. Experimental results produced a slope of -3.4 which adequately substantiates the existance of Rayleigh scattering. From 2-1 and the auxiliary equation

$$V = \frac{N_o}{N_p}\left(\frac{M}{2\rho A}\right) \qquad 2\text{-}2$$

where N_o is the total number of oxygen atoms per cm^3, M the molecular wright of SiO_2, ρ the density, and A avogradro's number, the number of scattering centers, Np can be calculated. The number of oxygen atoms per cluster, No/Np, is obtained and from the assumption of spherical particles he calculates the diameter of scattering to be 0.1μ. This value is consistant with the magnitudes observed by Debye and Lederhandler from angular dependence scattering experiments.

Schwuttke's work produces the most conclusive and significant information about the distribution of oxygen in silicon. He calculated that a minimum of 10^{10} oxygen atoms per cm^3 was necessary to produce scattering. This was confirmed by observations with his integrating sphere technique. An investigation was then conducted to determine the distribution of the oxide in the crystal. By application of etch-pit counts, decoration and light scattering techniques to the same specimens he was able to make observations of the effect of dislocations upon the oxide particles. It was found that in decoration by copper atoms, the precipitation is influenced by the oxygen content of the crystal. This suggests that oxygen is present in the dislocation networks and acts as nucleation centers for the copper precipitates. The copper prefers regions of high oxygen content thus delineating high density oxide clusters. Dislocations offer favorable sites for SiO_2 clusters. In relatively dislocation free crystals, clustering by heat treatment tends to take place in the bulk of the crystal.

5. Summary - From the foregoing review the following conclusions are presented:

1. Dislocation networds will produce incoherent infrared scattering and allow one to make qualitative conclusions about their distribution and size.

2. The assumption of a spherical shaped particle size for dislocation regions is not necessarily valid. Decorating techniques suggest a fishnet structure with a particle shape approaching thin platelets.

3. Particles formed by dislocation networks have some degree of preferred orientation.

4. Oxygen tends to concentrate on dislocation sites. Heat treatment at 1000°C produces higher concentrations of SiO_2 on these sites through clustering. This constitutes an increase in particle size.

5. In crystals of low dislocation density, SiO_2 molecules will cluster in the body of the crystal. Assumptions of a spherical cluster shape are not substantiated.

6. Dislocations and oxide impurities of appropriate size are present to cause incoherent scattering.

7. Direct evidence exists of dislocation loops as large as 50μ in diameter. Strong indications exist for sizes as small as 1μ diameter.

CHAPTER III

THEORY OF SMALL-ANGLE SCATTERING OF X-RAYS

A. General - The purpose of this study is to investigate the feasibility of applying small-angle scattering techniques to the determination of dislocation networks or impurity concentrations in silicon crystals. These heterogeneities constitute a particle distribution within the material. Therefore, it is appropriate that a review of the theory of small-angle scattering by particles be presented at this point.

The early theory was primarily developed on a qualitative basis by Guinier[13,14] and later extended to yield more quantitative results by Guiner and Fournet[15]. Small angle scattering is a phenomenon commonly observed with visible light. The halo observed around the moon due to scattering of the light by small mist droplets is the result of small angle scattering. To observe such an effect, the size of the scattering particles must be of the order of ten to a hundred times the size of the wavelength of the scattered light. For this type of scattering the following approximate relationship is observed:

$$\epsilon = \frac{\lambda}{d} \tag{3-1}$$

in which ϵ is the angle of diffraction, λ the wavelength, and d the mean diameter of the particles. The similarity between this relation and Bragg's Law,

$$\lambda = 2d \sin \theta \tag{3-2}$$

is apparent. However, one must not associate this type of diffraction

with that produced by the regular periodic cyrstallites to which Bragg's Law is applied. It is, in fact, the very nature of the variation, or non-periodicity of structure which gives rise to the small angle scattering to which the theory will be applied. Guinier extended the relationship in equation (2-1) to include the same type of diffraction phenomenon in the region of X-rays. If the wavelength and particle diameter were both reduced in the same proportion, particles of the order of ten to a hundred angstroms should likewise produce detectable small angle scattering.

X-rays are scattered by the electrons of the diffracting medium. Ordinary X-ray patterns are obtained from the scattering of electrons of atoms situated at regular coherent lattice points. However, low-angle scattering depends only upon the external dimensions of the particle, that is, the contour of the change in election density and not its internal structure. The X-ray diffraction of this type ordinarily observed is of the form of continuous scattering at angle of two degrees and below.

B. Theory - In order to make application of the phenomena to the determining of particle size, a relationship between scattered intensity and angle containing some dimensional parameter characteristic of the particle must be developed. This parameter obviously must be sensitive to the difference in the electron density due to the inhomodenity created by the particle. The derivation of appropriate formulas will be found in Appendix I, and only the results presented below. The characteristic particle dimension is designated by the symbol R. It must be dependent upon the electron distribution which in turn is a function of the atom distribution within the particle. The total number of scattering points is therefore N atoms times the atomic number. The relative displacement

of these points from some reference, in particular the center of gravity, is of interest. Take R^2 as the mean of the squares of the distances of each atom from the center and attach to it a value equal to its atomic weight. The value of R then is exactly that quantity in mechanics called the radius of gyration. It is a distance such that $MR^2 = I$ where M is the particle mass and I its moment of inertia relative to the center of gravity. This parameter therefore is only an indication of mass distribution and not shape. It is because of this very point that the basic theory still leads to only qualitative or semi-quantitative results. The majority of Guinier's later work[15] was devoted to the refinement of this aspect.

Appendix I yields the relationships:

for orientated particles . . . . . .

$$I/I_e = Nn^2 \exp\left(-\frac{4\pi^3}{\lambda^2} R^2 \epsilon^2\right) \qquad (3\text{-}3)$$

for randomly orientated particles . . . . . .

$$I/I_e = Nn^2 \exp\left(-\frac{4\pi^3}{3\lambda^2} R^2 \epsilon^2\right) \qquad (3\text{-}4)$$

in which I = scattered intensity over an angle ϵ (in radians)

I_e = the scattering intensity by one electron (obtained by Thomson's formula)

N = the number of particles

n = the difference in the number of electrons in the particle and an equal volume of the external medium.

Taking the logarithom of each side of(2-3)one obtains:

$$\text{Log}_{10} I = \text{Log}\ Nn^2 I_e = -\frac{4\pi^2}{\lambda^2}\ \text{Log}_{10} eR^2 \epsilon^2$$

A plot of $\text{Log}_{10} I$ vs. ϵ^2 should yield a straight line for small values of ϵ^2, its slope, m, being $-4\pi^2/\lambda^2 \text{Log}_{10} e R^2$. This yields a value of

$$R = \sqrt{\frac{\lambda^2 m}{4\pi^2 \text{Log}_{10} e}} = .0765 \lambda \sqrt{m}$$

for orientated particles and $.418 \lambda \sqrt{m}$ for randomly orientated particles. Usually one plots $\text{Log}_{10} I$ as a function of the square of the magnitude of the vector h, where:

$$|h| = \frac{4\pi \sin\theta}{\lambda} \simeq \frac{2\pi\epsilon}{\lambda}$$

for small angles
(θ = 1/2 the scattering angle)

C. Interpretation of results - A straight line curve predicted by equations (3-3) and (3-4) is seldomly obtained in practice. To obtain a strictly linear curve demands only one discrete particle size and of course good precise experimental data. Figure 3-1 is a good example of these conditions for a solution of albumin. The radius of gyration is obtained from the slope of the linear plot. From other information about the particle such as the density, modecular weight, and chemical structure, R can be transformed into a particle shape with specific dimensions. Now take the case presented in Figures 3-2 and 3-3. What statements can be made about particle sizes for these experimental data? The theory of small angle scattering exhibits its greatest validity for particles of dilute concentrations. This is due to the basic hypothesis that it is the difference in electron density of the particle and the medium upon which such scattering depends. For increasing concentrations and orientations a point is reached in which there appears to be a degree of long range order and particle interference. This tends to create a step or

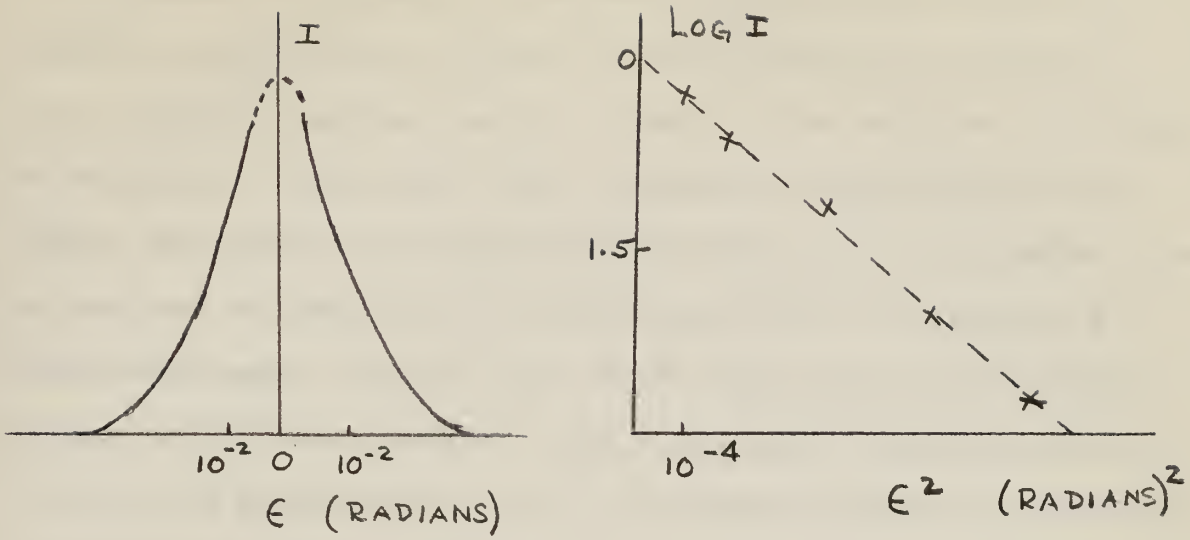

Fig. 3-1 Low angle scattering of a solution of albumin, after Guinier[2]

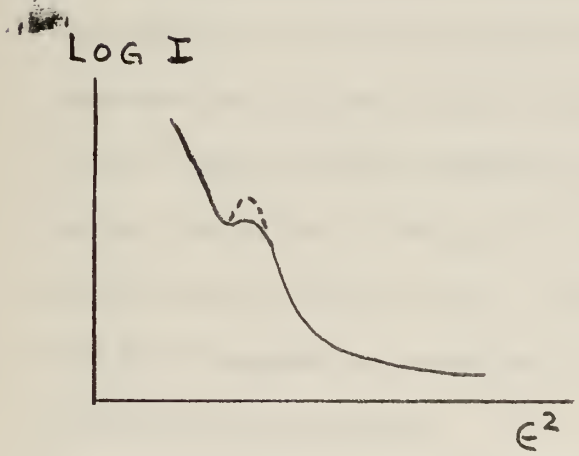

Fig. 3-2 Particle interference

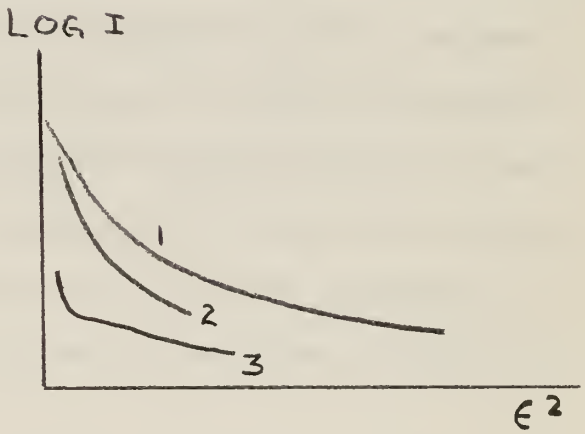

Fig. 3-3 Mixtures of particle sizes

even a maxima in the otherwise continuous scattering curve. Figure 3-2 represents this situation. The most representative of scattering patterns is represented in Figure 3-3. Only qualitative information can be obtained from these curves. In curve 1, the variation of the slope at low angles is sufficiently small to permit an extrapolation to the origin. The slope at the origin gives an average radius of gyration. One can say that the sample does not contain particles of too large an R to escape measurement. Curves 2 and 3 do not permit such an extrapolation. The conclusions to be made are: Curve 2, the sample contains many large particles and few small ones; Curve 3, the sample contains some very large particles but not many small ones.

Guinier[15] and Debye[16] extend the theory in an attempt to interpret quantitatively curves exhibiting mixtures of particle sizes. His analysis is based upon distribution functions in which he applies Maxwellian distributions. A more straight-forward graphical procedure has been developed by Jellinek, Solomon and Frankuchen[17] in which the contributions of particle size groups are successively subtracted out of the curve. The curves of Figure 3-3 represent such a sum of the contributions of many particle sizes. They point out that the scattering of X-rays by a homogeneous assemblage of spherical particles of radius R can be given by the equation,

$$I(\theta) = CWR^3 e^{-0.221 h^2 R^2} \qquad (3.5)$$

where I is the scattered intensity as a function of θ (half the scattering angle), $h = \frac{4\pi \sin\theta}{\lambda}$, W is the weight of the specimen doing the scattering and C is a constant for a given material. The distribution of particle sizes may be represented by the function W(R) where W(R) is

the weight fraction within the sample of radius R. Summing the total scattered intensity leads to the expression for the curve:

$$I(\theta) = C\int_0^{\infty} W(R) R^3 e^{-0.221 h^2 R^2} dR \qquad 3\text{-}6)$$

The curve of Log I (θ) vs. h^2 will, at the higher values of h^2, yield a slope representing a single value function of R and with an intercept equal to CWR^3. Equation (2-6) suggests possibilities of obtaining W(R) as a continuous function of I(θ) by application of the Fourier transform method. A treatment of this analysis is given by Bauer[18] involving a great detailed process. The Jellinek, Solomon, and Frankuchen method greatly simplifies matters by obtaining in place of the continuous function of W(R) a graphically obtained set of discrete fractions of W(R) over the observed range. Their data and graphical analysis for alumina gel are presented in Figure 3-4. The tangent to the curve at the greatest observed angle of scattering is taken and extrapolated back to the ordinate as the intercept K_1. A point by point subtraction of the tangent from the curve yieldsthe new curve (dashed in the figure). This represents the scattering contributed by all particles of size larger than the value yielding slope m_1. From this curve the tangent m_2 is taken and the intercept K_2 is obtained. The process is repeated until extrapolation and point by point curve subtraction is no longer feasible. The slopes are calculated and from an appropriate graph of slope vs. R (Jellinek, Solomon and Frankuchen)[19] the discrete radii are obtained. Since the intercepts are proportional to $R^3W(R)$, the quantity K_i/R_i^3 represents the fraction of the i^{th} particle contained within the sample. The complete calculation for carbon black is presented in Table 1.

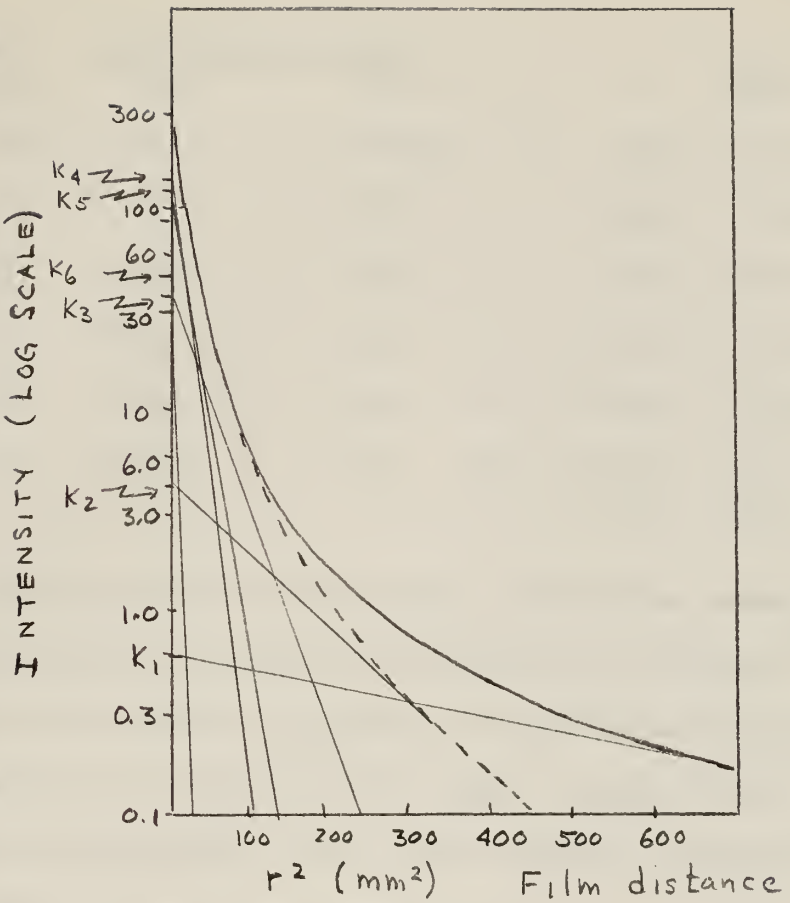

Fig. 3-4 Plot of $\text{Log}_{10} I(\theta)$ against r^2 for Alumina Gel. Jellinek, Solomon, and Frankuchen, Ind. Eng. Chem. Annual Ed., 18, 172 (1946).

TABLE I

Calculation of Particle Sizes from Small-Angle Scattering Data for Alumina gel (Jellinek, Solomon, and Frankuchen[7])

	Ordinate Intercept	Calculation of Slope							
		log I	r^2	log I	r^2	R	R^2	$K/R^3 \times 10^4$	Weight Proportion
K_1	0.61	0.484	630	0.000769	10	1,000	6.10	0.194	
K_2	4.3	1.633	457	0.00358	22	10,600	4.06	0.129	
K_3	39	2.591	240	0.0108	37	50,600	7.71	0.245	
K_4	115	3.061	140	0.0219	54	157,000	7.32	0.232	
K_5	140	3.146	107	0.0294	62	238,000	5.88	0.186	
K_6	48	2.681	33	0.0812	103	1,092,000	0.44	0.014	
						Total	31.51	1.000	

Jellinek et al in their original publication acknowledged the apparent empirical nature and only piecewise continuous size distribution of this method of analysis. They could only defend its validity by stating that it works for the systems (alumina gel and carbon black) to which it was applied. In a later analysis of alumina gel[20] they were unable to obtain consistent results.

Bragg, Corwin and Buttrey[21] investigated mixtures of silica sols of two known particle diameters in an attempt to verify methods of particle size distribution. They were able to substantiate the prediction that the scattering at small angles arises predominantly from the larger particles and that the smaller ones control the scattering at larger angles. The application of Jellinek's graphical analysis was unsuccessful in reproducing the known particle sizes introduced. They state, however, that much of their scattering data was obtained at values of h beyond

which the Guinier approximation is valid. A method due to Porod which relates scattering at larger angles and total surface area was also applied. Porod predicts the following relationship:

$$I(h) = 2\pi \rho^2 S/h^4 \qquad (3\text{-}7)$$

in which ρ is the mean electron density, S the total particle surface area and h as previously defined. In collimating systems of large slit widths, the quantity h^4 is replaced by h^3. A plot of ln I vs ln h should yield a straight line of slope equal to -3 (using h^3) and intercept of $2\pi \rho^2 S$. For spherical particle disperse system the geometrical relationship $R = 3V/S$, where V is the particle volume, obviously holds. An analogous surface averaged particle radius can be obtained for polydispersed systems. The calculated radius favors those particles which make the largest contribution to the surface area.

The above survey substantiates Guinier's original prediction that the application of small angle scattering in obtaining accurate quantitative results is indeed limited. For widely separated spherical particles of one diameter, exact sizes can be measured. Non-spherical particles can be quantitatively investigated if complementary information such as volume, surface area, and molecular weight are known. Mixtures of sizes and/or unknown shapes lead to qualitative results of widely varying validity depending upon the means of analysis employed.

CHAPTER IV

APPLICATION OF SMALL-ANGLE INFRARED SCATTERING TO PARTICLE SIZE IN SILICON CRYSTALS

A. General - Guinier developed his theory of small-angle scattering by an extension of the classical theory of atmospheric scattering of visible light down to the region of X-rays and particles of comparable size. It therefore seems reasonable that a similar extrapolation can be made toward the region of the infrared spectrum and particle dimensions of the order of microns. The limitation to materials which are relatively transparent to infrared radiation is obvious. An inspection of equation (3-1), $\epsilon \simeq \frac{\lambda}{d}$ suggests two possibilities. One might attempt to increase the wavelength, maintaining a given particle size, and thus obtain scattering at larger angles. This would eliminate the complexities associated with small angle cameras and diffraction techniques. However, in the case of X-rays, longer wavelengths are increasingly attenuated by matter. This introduces problems associated with reduced intensities. The theoretical limitation placed upon this first alternative is that the expressions developed in the small-angle theory are derived using an approximation called the "law of Guinier". Equation (3-3) and (3-4) for the scattered intensity contain the term $e^{-KR^2\epsilon^2}$ in which K represents $\frac{2\pi}{\lambda}$. As shown in Appendix I this exponential is an approximation of the series

$$e^{-KR^2\epsilon^2} = 1 - KR^2\epsilon^2 + \frac{K^2R^4\epsilon^4}{2} - \frac{K^4R^8\epsilon^8}{6} - \cdots\cdots\cdots$$

The approximation coincides with the exact expression only up to the 4th power of h. Therefore, for large h, the relationship

$$I/I_e = N n^2 e^{\frac{-4\pi}{\lambda^2} R \epsilon^2}$$

is no longer valid. In fact, the Guinier analysis breaks down for $hR \leq 1$. The above approximation is the law of Guinier. Therefore, one cannot increase the wavelength in an attempt to obtain scattering at larger angles and still apply Guiner's small-angle scattering theory.

The other suggested possibility as previously mentioned is that of increasing both λ and d, maintaining the same proportion. In this manner, the angle limitation placed upon ϵ is not exceeded and larger size particles can be measured. The study of silicon heterogeneities will be directed toward using this relationship.

Kaiser, Keck and Lange[22] were able to show by means of a 9.1 micron wavelength absorption band the existance of SiO_2 clustering in silicon crystals. In Chapter II it was pointed out that Schwuttke was able to make some semi-quantitative conclusions of oxygen impurity clustering and dislocation networks in silicon by infrared scattering. Debye and Lederhandler[23] stated that they were able to obtain information on SiO_2 particle size in silicon by measuring the angular distribution of infrared scattering. None of the above investigators were able to establish a discrete particle size.

The problem of interpretation of scattering data still remains open. With what kind of particle shape can one associate dislocations? Can SiO_2 clustering be considered to consist of spheroids, elipsoids or platelets? There is strong indication that oxygen precipitation occurs

along dislocation networks outlining a stringy network, or possibly, along rods of an average diameter but "infinite" length.

B. Dislocations - Dash's decorating techniques allows one to draw some conclusions about dislocation networks. Grown-in dislocations tend to form in favorable orientations. The formation of a hexagonal structure in the (111) plane by the intersection of edge dislocations and screw components was pointed out in Chapter II. Plastic deformation induces dislocation loops from Frank-Reed sources in the (111) plane. Networks of loops ranging from 2 to 50 microns in diameter were detected. These observations suggest the use of equation (3-3) for orientated particles for low angle scattering analysis. The fulfillment of the widely separated particle criterion can be assured by an inspection of the scattering profile. A dense system will exhibit particle interference and a drop off in intensity at zero angle. A mixture of sizes will be indicated by the concave upward nature of the plot of Log I vs ϵ^2.

The extension of small-angle scattering theory to the measuring of dislocations networks offers one gross possible shortcoming. The scattering is due to the difference in the electron density of the particle and the surrounding medium. Does a dislocation meet the description of a particle in this aspect? Dislocations by definition do represent discontinuities in atomic structure. This represents only a variation in electronic density covering a magnitude of only atomic distances. However, there is a stress field surrounding the core which falls off according to $1/r^2$; r being the distance from the core. Compared to the magnitudes of atomic forces, this may be considered as a relatively

long range force. From the consideration of Hooke's Law, this stress is only a manifestation of atomic displacements. Cottrell[24] indicates that one-half of the total strain energy surrounding a dislocation lies within a region near the core. This offers possibilities of contributing sufficient variation in the electron density to affect scattering of the infrared radiation. Furthermore, Guinier emphasized that "the low-angle scattering depends on the external dimension of the particle and not on its internal structure." One can thus draw the conclusion that a network of dislocations warrants the description of a group of particles.

As reported in Chapter II, Schwuttke has reported the detection of infrared scattering in silicon crystals containing dislocation densities of at least 10^8 per cm^2. This observation favorably supports the "particle nature" of dislocation networks suggested above.

C. Oxygen Impurities - As previously noted in Chapter II, oxygen exists as clusters in silicon in the form of SiO_2. Schwuttke reported scattering in crystals containing at least 10^{17} oxygen atoms per cm^3. Kaiser reported Rayleigh scattering at concentrations of $5X10^{10}$ scattering centers (10^{18} oxygen atoms) per cm^3. Both investigators made the assumption that the SiO_2 clusters are spherical in shape. This assumption has not been verified. A great deal of evidence leads one to believe that precipitation of the oxide occurs at dislocation sites as do the copper atoms observed in Dash's decorating technique. Microscopic examination fails to reveal the presence of a separate SiO_2 phase. This however only serves to insure that clusters greater than approximately 0.1-1 micron do exist. Submicroscopic spheriodal particles

and dislocation site precipitates could still be formed. The existance of submicroscopic spheriodal clusters would obviously be most favorable to the small angle scattering method. They would tend to be nearly uniform in size and widely separated in distribution. All three of these conditions (spherical, uniform, dilute) characterize the optimum conditions for the application of the Guinier analysis.

The alternative of the diffusion of oxygen to dislocation sites still exists. It is known that dislocation sites play a significant role in the nucleation of precipitates.[25] The problem reduces to: once nucleation has commenced, what shape do the particles take? Continuous precipitation along dislocation lines establishes the same question of meeting the particle criterion as discussed in section B.

The foregoing discussion presents strong evidence of the applicability of small-angle infrared scattering techniques to silicon crystals. With the appropriate complimentary information, a good estimate of particle size and distribution should be obtained. Chapter VI will be devoted to the analysis of experimental data by use of the ideas presented here.

CHAPTER V

EXPERIMENTAL PROCEDURE

A. Specimen preparation - A 1.5 cm. diameter silicon single rystal was obtained from the Shockley Transistor Laboratory. This crystal was grown in the ⟨100⟩ direction and measured 10 ohm-cm resistivity. Several slices ranging from 1.5 to 6 mm. were cut perpendicular to the growth axis and polished by standard metallographic procedures to minimize surface scratches and pitting. A check of the finish at 400 X magnification revealed a relatively small density of surface pitting.

It was initially anticipated that absolutely parallel plane surfaces would be necessary in order to obtain consistant results. Repeated attempts were unsuccessful in cutting parallel faces. It was decided that a small amount of wedge could be tolerated if its gradient is parallel to the plane of detector rotation. If the taper were not in the plane of rotation, the refracted beam would contain a vertical component which would vary across the face of the radiation detector. A taper in the plane of rotation merely caused a refraction which established the non-diffracted or "zero angle" beam, I_o, at a point other than directly in line with the incident rays. Accordingly, the crystals were mounted and orientated by use of an optical gonimeter. The measured deviation from parallel averaged about 1 degree. This amount of wedge was checked by means of the infrared beam using the relationship for minimum deviation of refracted light. For minimum deviation:

$$n = \frac{\sin \frac{1}{2}(\alpha + \delta_{min})}{\sin \frac{1}{2}\alpha}$$

n = index of refraction of the silicon for the wavelength used (3.449 for λ = 2.3) 26

α = angle between crystal faces.

δ_{min} = deviation angle.

The refracted angle, δ_{min}, as measured by peaking intensity, agreed to within 10' arc of the value determined by the optical goniometer.

B. Optics - A photograph of the experimental set-up appears in figure 5-1. The basic instrument is an American Optical Company table spectrometer which had previously been modified for use as an optical gonimeter. In an instrument used to measure small angle scattering there is a problem of achieving adequate intensity without excessively sacrificing resolution. One must make a decision as to the poorest acceptable resolution and then strive to obtain sufficient intensity consistant with the sensitivity of the detector and radiation source. Two pairs of slits were used; one pair to collimate the incident beam and one pair to shield the detector from all radiation other than the transmitted diffracted beam. Slit separation was limited to 13 cm. by the collimator barrels of the spectrometer. Initially, the source of radiation used was a carbon arc. The carbon arc is a rich source of near infrared, but difficulty was encountered in maintaining a stable, well defined vapor crater which created alignment problems. A zirconium arc was then substituted for the carbon arc with a moderate decrease in intensity but considerable gain in stability. Several runs were made at varying slit openings and an acceptable signal was obtained with a width of 0.79 mm.

The wavelength employed was governed by the optical transmission of silicon and the type of detectors available. Figures 5-2 and 5-3 represent

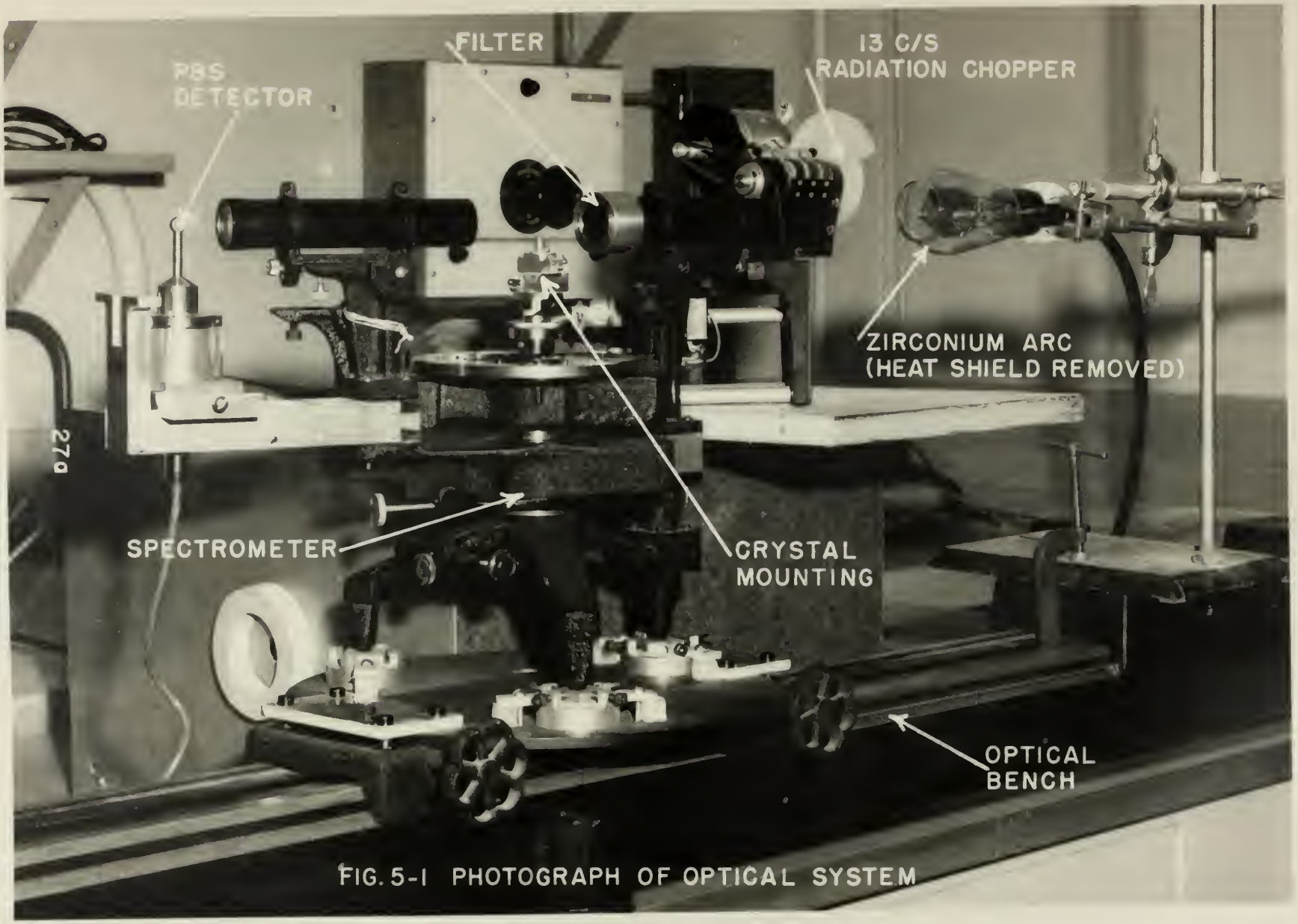

FIG. 5-1 PHOTOGRAPH OF OPTICAL SYSTEM

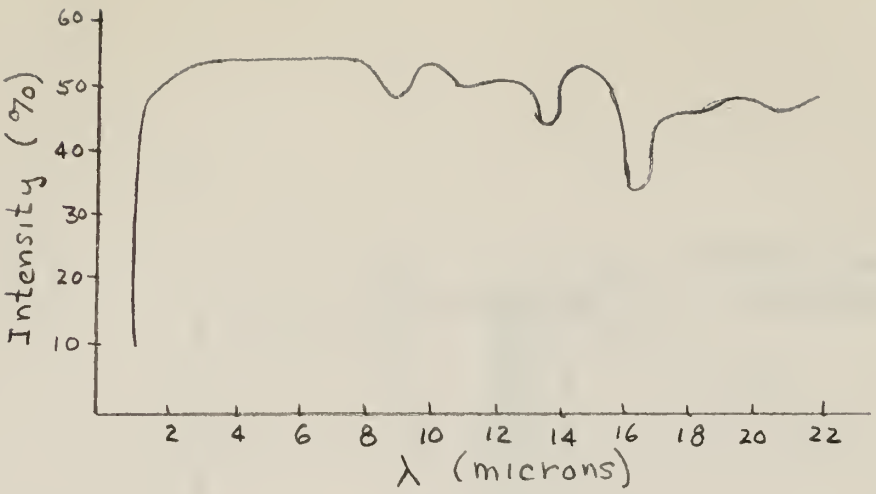

Fig. 2-2 Transmission properties of silicon, ρ = 150 Ω-cm, thickness 0.5 mm
After Smith, Jones and Chasmar[27]

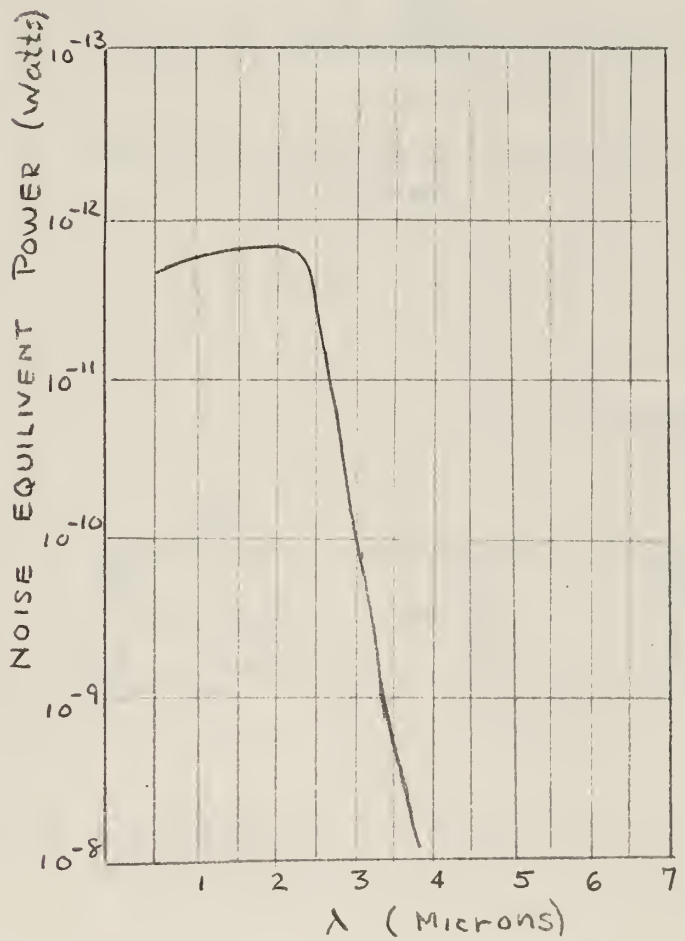

Fig. 2-3 Optimum NEP vs. Wavelength for PbS Detector at 25°C

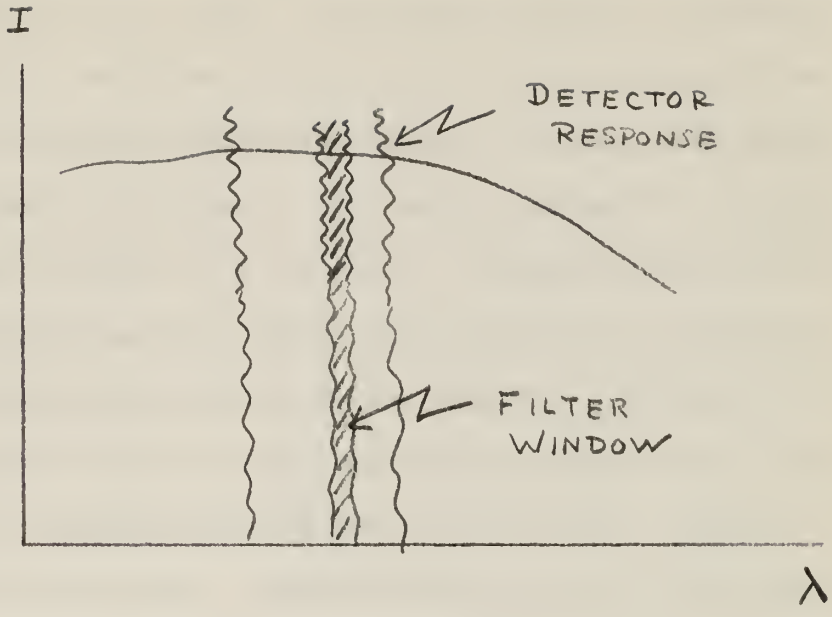

Fig. 5-4 Illustration of decrease in power incident upon detector

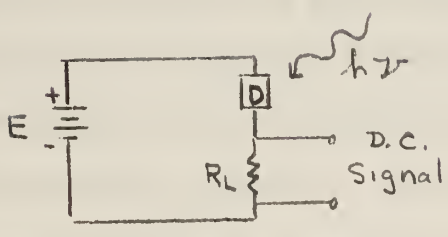

Fig. 5-5 Photoconductor Circuit d c.

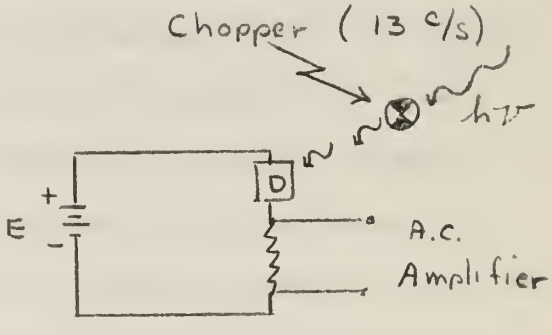

Fig. 5-6 Photoconductor Circuit a.c.

the factors governing the wavelength selected. A wave length of 2.3 microns was decided upon because of the high peaking sensitivity of PbS photo-conductors at this wavelength. This choice is consistant with the broad transmition band of silicon in the near infrared region. The beam was monochromated with a "spike" interference filter. As previously mentioned, obtaining sufficient intensity in the beam was a problem. Figure 5-4 shows how the total diffracted energy is successively diminished from that of the initial source. The energy radiated is represented by the area under the curve of $I = F(\lambda)$. A detector responds to total energy received within the range of its sensitivity. The filter greatly diminishes the energy received by the detector. Additional reductions in energy are caused by components in the optical train. The The filter transmits only approximately 80% of the incident radiation at the center of the wave length. Another fraction of this transmitted beam is absorbed by the crystal.

An attempt was made to increase the light intensity by concentrating the beam with a lens system. It was suspected that the added attenuation due to the glass optical elements would be more than offset by the beam concentration. Also, if the system were successful, NaCl or KBr lenses could be substituted for glass, thus reducing the attenuation. The focusing of the light with lenses did increase the detector response. However, this gain was obtained at the expense of collimation and associated directional resolution. One cannot increase the energy radiated per area and still maintain parallel rays. In brief, the parallel rays cannot be squeezed closer together to increase the photon density. To do so would appear to be contrary to the second law of thermodynamics. A lens

system would serve only in moving the position of the source as a matter of convenience. The source has a finite size and cannot be concentrated. Therefore, an increased signal was obtained through increased slit width and moving the source as close as practicable, consistant with adequate resolution.

C. Electronics - Associated with the problem of the low intensity was the problem of signal amplification. Figure 5-5 is a schematic sketch of a typical detector circuit. In photoconducting cells, it is necessary to pass a direct current through them in order to record the change in resistance due to photo-conductivity. Maximum sensitivity is obtained in PbS cells with an applied voltage of the order of 100 volts. "Dark" resistance of a photo-conductor is usually 1 megohm. For a maximum transfer of power, the output or load resistor R_L should be matched to the detector resistance and thus also 1 megohm. This creates a voltage divider providing approximately 50 volts across the load resistor. With the small signals obtained, of the order of millivolts, it was not possible to separate the variation in voltage from the voltage measured. Increasing the load resistor or using d.c. amplifiers merely increased the V along with V maintaining the same ratio. Direct current amplifiers have been used with PbS cells with large signals but not of the order of magnitude encountered in the experimental setup. Separation of the detector signal from the steady d.c. bias can be achieved by use of chopped radiation as indicated in Figure 5 6 An a.c. amplifier is used to amplify the a.c. component created by the chopper. Amplifier units were obtained from a Perkins-Elmer infrared spectrometer. Essentially, all the components except for the optical train were easily adapted for use in an infrared diffraction system. The units consist of a 13 cycle per second

chopper, pre-amplifier, 13 cycle per second amplifier with rectified output, and a Leeds and Northrup recorder. With proper shielding of the detector, a high signal to noise ratio was obtained and relatively low intensity signals adequately amplified.

CHAPTER VI

EXPERIMENTAL RESULTS

Scattering data were obtained for three slices of the original crystal. Thicknesses were 2, 3, and 6 mm. Dislocation densities obtained by etch-pit counts were estimated to be 10^7-10^8 per cm^2 for each specimen. Since the first tests were conducted without heat treating the crystals, no contribution to the light scattering by oxygen was anticipated. Microscopic examination did not reveal the presence of a separate phase due to SiO_2 clustering or other impurities.

Figures 6-1 and 6-2 represent the plotted scattering data for the 2 mm and 6 mm specimens. The 3 mm crystal produced essentially identical data as the 2 mm specimen. The highest value of ϵ^2 correspond to a scattering angle of 2 degrees. Also indicated on each curve is the limit specifying $Rh \leq 1$. Therefore the data was obtained at angles well within those for which the Guinier analysis is applicable. A check was made for parasitic diffraction due to the collimating slits. This was performed with the optical arrangement identical to that of the test runs but without the crystal. The intensity was reduced to essentially zero at angles of 1 degree ($\epsilon^2 \simeq 4$). Sharp minima were observed at an angle of 40 minutes. This caused the discontinuity in the specimen scattering curves observed at values of ϵ^2 equal to 2-3. The main conclusion drawn from the parasitic diffraction test is the absence of any contribution to scattering in the region of interest, $\epsilon^2 > 4$, due to the slits.

From the limiting slopes, radii of gyration of 5.70 μ and 4.79 μ are calculated for the 2mm and 6 mm specimens respectively. To interpret these values in terms of a particle size auxiliary information of

particle shape is required. As pointed out in Chapter II, the results of earlier investigators suggest a polygonal or circular platelet configuration. The difference in electron density is concentrated about the periphery of the loop. A good approximation of particle shape would be that of an annulus with a radius of gyration of:

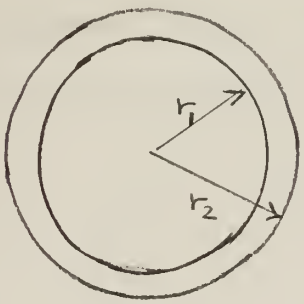

$$R_o = \sqrt{\frac{r_1^2 + r_2^2}{2}}$$

If the width of the dislocation line and bordering displaced atoms is considered to be narrow compared to the radius of the loops one can assume $r_1 \simeq r_2$. For this approximation, the expression reduces to:

$$r = R_o$$

In order to calculate a particle size, we must therefore assume that the particles are discs of negligible thickness whose radius of gyration is the effective radius in the plane of the disc. This assumption leads to a particle size with diameters of 11.40μ and 9.58μ for the specimens of figures 6-1 and 6-2 respectively. These figures are of the same order of magnitude of the values observed by Dash using decoration techniques. The resistivity measurement imply a considerable impurity content. The presence of oxygen will be seen at large values of ϵ^2. The results indicate no particles less than 11μ in diameter. We therefore conclude that the impurities are in solution in the silicon crystal or at most trapped in the dislocations.

Figures 6-1 and 6-2 indicate a distribution of particle sizes. The long linear portion of the slope at large angles describe a larger percentage of smaller particles. The sharp bend in the curve at small angles shown in figure 6-1 indicate a smaller proportion of large particles for the 2 mm specimen. However, the data at angles less than 1 degree are not completely reliable due to the contribution of parasitic scattering by the collimating slits.

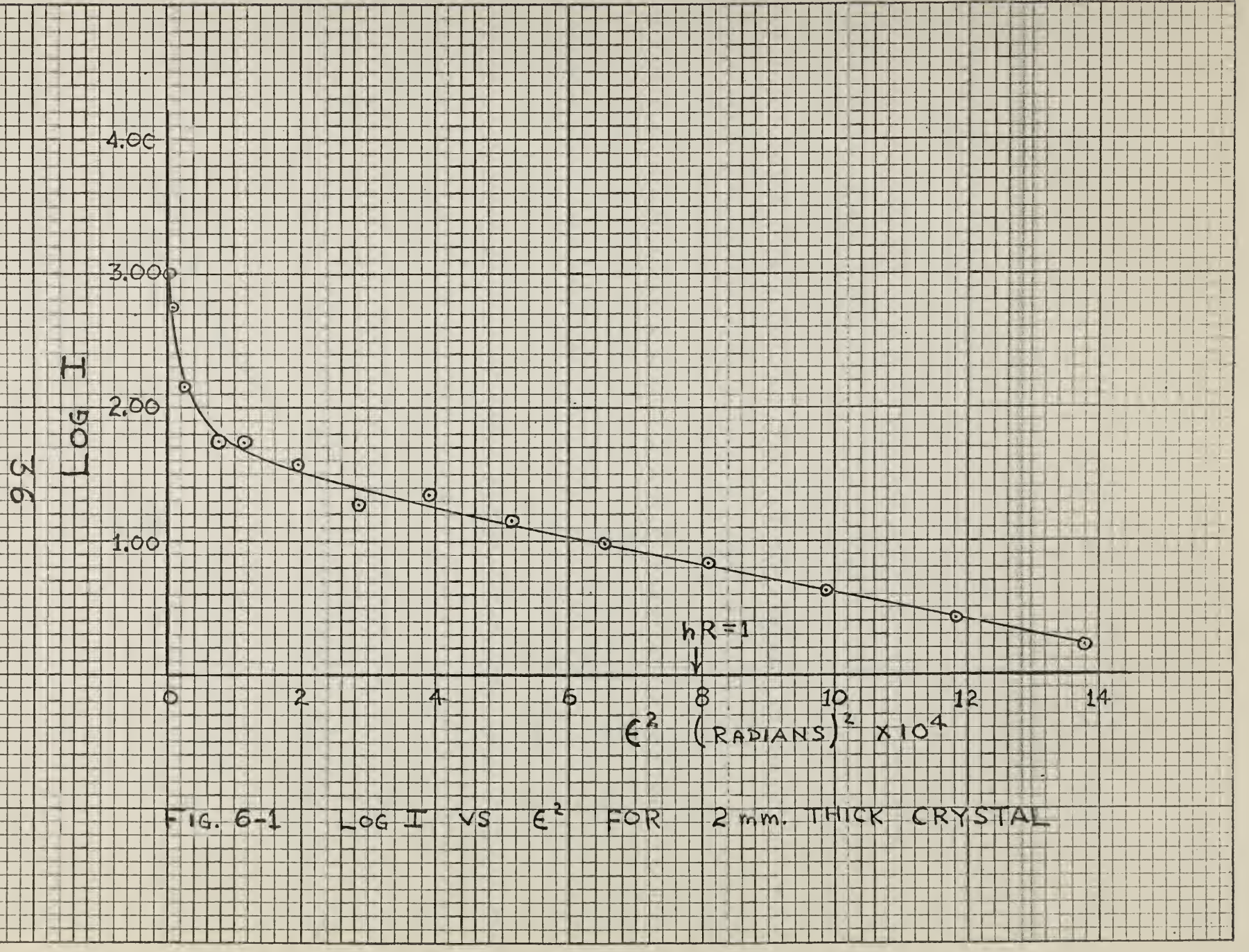

FIG. 6-1 LOG I VS ϵ^2 FOR 2 mm. THICK CRYSTAL

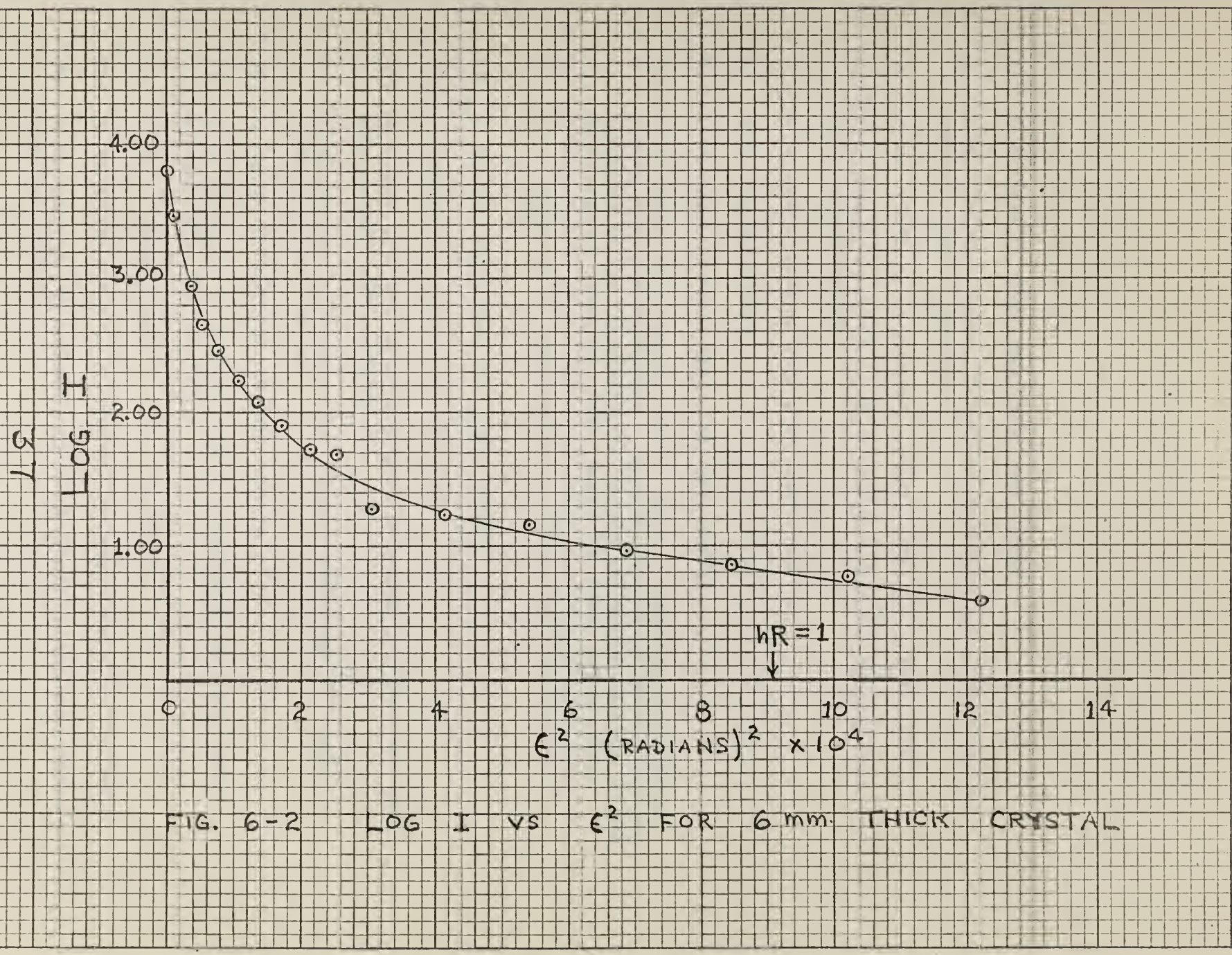

FIG. 6-2 LOG I VS ϵ^2 FOR 6 mm. THICK CRYSTAL

BIBLIOGRAPHY

1. W. R. Dash, Journal of Applied Physics, 27, 1193 (1956).

2. Ibid, 30, 459 (1959).

3. J. B. Newkirk, Phys. Rev. 110, 1465 (1958).

4. G. H. Schuttke, General Telephone and Electronics Laboratories Research Report TR60-300.7.

5. J. J. Gilman, W. G. Johnson, J. Appl. Phys., 27, 1018 (1956).

6. F. L. Vogel, W. G. Pfann, H. E. Corey, and E. E. Thomas, Phys. Rev., 90, 489, (1953).

7. W. R. Dash, J. Appl. Phys., 27, 1194 (1956).

8. Ibid, 30, 461 (1959).

9. A. R. Lang, J. Appl. Phys., 29, 597, (1958).

10. J. R. Patel, R. S. Wagner, and S. Moss. "Metallurgy of Elemental and Compound Semiconductors", Proceedings of a Technical Conference, sponsored by the Semiconductors Society and Boston Section, of the Metallurgical Committee, AIME, August 21, 1960, Boston, Mass.

11. P. P. Debye and S. Lederhandler, Am. Phys. Soc. Bul. Ser II, 2, 66, (1957).

12. W. Kaiser, Phys. Rev. 105, 1751, (1957).

13. A. Guinier, Ann. Phy., 12, 161 (1939).

14. A. Guinier, "X-ray Crystallographic Technology", Hilger and Watts Ltd., London, 1952, Chapter XII.

15. A. Guinier and G. Fournet, Small Angle Scattering of X-rays", Wiley, New York, 1955.

16. P. Debye, J. Appl.Phy. 29, 679, (1957).

17. M. J. Jellinek, E. Solomon, and I. Frankuchen, Ind. Eng. Chem. Analytic Ed., 18, 172 (1946).

18. S. H. J. Bauer, Chem. Phy. 13, 450 (1945).

19. M. H. Jellinek and I. Frankuchen, Ind. Eng. Chem. 37, 158 (1945).

20. M. H. Jellinek, E. Solomon, and I. Frankuchen, Ind. Eng. Chem., 41, 2259 (1949).

21. R. H. Bragg, I. Corwin, and J. W. Buttrey, J. Appl. Phys., 31, 1183, (1960).

22. Kaiser, Keck, and Lange, Phy. Rev., 101, 1264 (1956).

23. P. P. Debye and S. Lederhandler, Bul. Amer. Phy. Soc., Ser. II, 2, 66, (1957).

24. A. H. Cottrell, "Dislocation and Plastic Flow in Crystals", pp 38, Oxford, London (1956).

25. Pearson, Read, and Feldman, Bull, Am. Phys. Soc. Ser II, 1, 295, (1956).

26. H. B. Briggs, Phy. Rev. 77, 287, (1950).

27. J. B. Smith, F. E. Jones, and R. P. Chasmar, "The Detection and Measurement of Infra-Red Radiation", Oxford, London, (1957).

APPENDIX I

DERIVATION OF SMALL-ANGLE SCATTERING FORMULAS

A. Scattering By Several Waves

A sinusoidal wave, of frequency ω, is defined by its amplitude A and phase ϕ :

$$a = A \cos(\omega t + \phi)$$

This can be expressed in complex variable notation:

$$u = A e^{j(\omega t + \phi)}$$

in which a is the real part of u. For several waves of same frequency propagated in the same direction the observed amplitude will be the sum of the amplitudes of each individual wave.

$$U = \sum u_i = e^{j\omega t} \sum A_i e^{j\phi_i}$$

The resultant amplitude and phase can be obtained by vector addition from the following diagram:

Fig. I-1

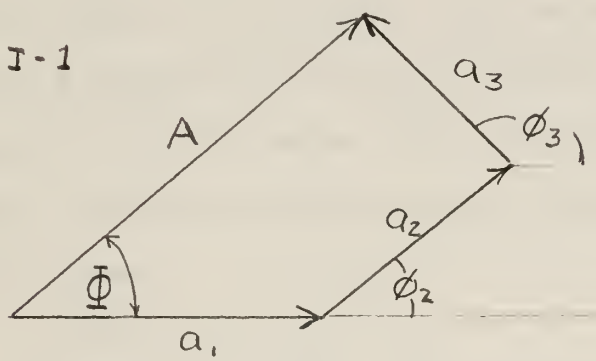

Since the intensity, I, is equal to the square of the amplitude, it is evident from the above diagram that:

$$I = \left(\sum A_i \cos \phi_i\right)^2 + \left(\sum A_i \sin \phi_i\right)^2$$

Expressed in complex variable notation:

$$I = U \times U^* = \left(e^{j\omega t} \Sigma_i A_i e^{j\phi_i}\right)\left(e^{-j\omega t} \Sigma_k A_k e^{-j\phi_k}\right)$$

$$= \Sigma_i \Sigma_k A_i A_k e^{j(\phi_i - \phi_k)} = \Sigma_i \Sigma_k A_i A_k \cos(\phi_i - \phi_k) \qquad I-1$$

B. Phase Difference of Waves Scattered by Two Electrons

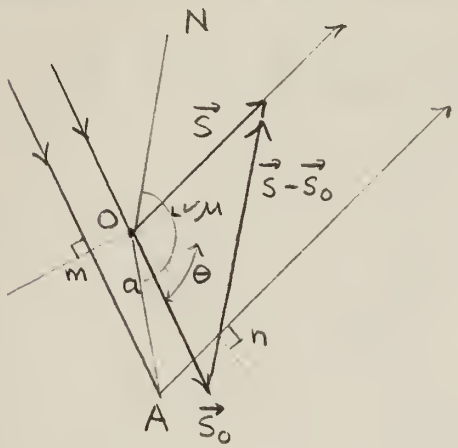

Fig I-2

In the above figure, $\vec{S}_o$ represents a unit vector along the incident rays. Points O and A represent two electrons scattering the incident rays. $\vec{S}$ is the scattered ray unit vector. The phase difference between the rays scattered at O and A can be represented by the retardation distance MA + An.

From vector algebra:

$$|mA| = \vec{OA} \cdot \vec{S}_o$$

$$|An| = \vec{OA} \cdot -\vec{S}$$

$$|mA + An| = \vec{OA} \cdot (\vec{S}_o - \vec{S})$$

The phase difference is therefore:

$$\phi = \frac{2\pi}{\lambda} \vec{OA} \cdot (\vec{S}_o - \vec{S})$$

Since $|\vec{S}_o - \vec{S}|$ is equal to $2 \sin\theta$ and is parallel to ON,

$$\phi = \frac{4\pi}{\lambda} a \sin\theta \cos\mu \qquad (I-2)$$

C. Intensity of Low-Angle Scattering by Small Particles

1. Oriented particles. The intensity of the scattering by an individual atom is $I_e f$ where I_e is the intensity of the scattering by one electron and f the atomic scattering factor. The amplitude is then represented by $A = \sqrt{I_e f}$ and formula (I-1)can be written:

$$I = I_e \Sigma_k \Sigma_i f_i f_k \cos(\phi_k - \phi_i)$$

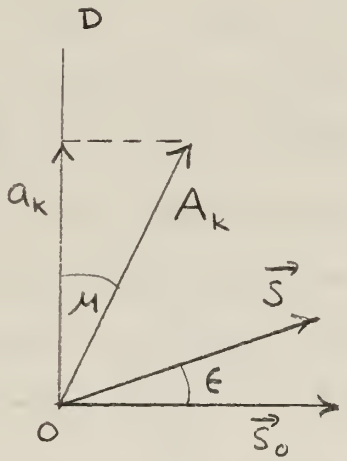

Fig. I-3

In figure I-3, ϵ represents the scattering angle and is equal to 2θ. Since the scattering considered here is at very small angles, OD may be regarded as perpendicular to $\vec{S}$ for all values of ϵ . The length a_k is the projection of A_k on ON. Therefore the phase difference, formula (I-2), can be written:

$$\phi_k = -\frac{2\pi}{\lambda} \epsilon \cdot \overline{OA_k} \cos\mu = -\frac{2\pi}{\lambda} \epsilon \cdot O a_k$$

and

$$I = I_e \Sigma \Sigma f_i f_k \cos\left(\frac{2\pi}{\lambda} \epsilon \cdot \overline{a_k a_i}\right).$$

Letting $\overline{a_i a_k} = l_{ik}$ and $\frac{2\pi}{\lambda}\epsilon = h$, the intensity can be expressed as a cosine series:

$$I/I_e = \left(\Sigma f_k\right)^2 - \frac{h^2}{2} \Sigma_i \Sigma_k \left(f_i f_k l_{ik}\right)^2 + \frac{h^4}{24} \cdots\cdots$$

The various scattering points, a_1, a_2,---a_p can be projected on the normal OD as X_1, $X_2 \ldots X_p$. Hence

$$l_{ik} = X_k - X_i$$

The double summation $\Sigma_i \Sigma_k f_i f_k (l_{ik})^2$ summed first over k is:

$$\Sigma_k f_i f_k (l_{ik})^2 = f_i \Sigma_k \Sigma_i x_k^2 - 2 f_i x_i \Sigma_k f_k x_k + f_i x_i^2 \Sigma f_k$$

Choose the origin such that $\Sigma f_k x_k = 0$. This represents the projection of the center of gravity of the particle on OD. The second summation gives:

$$\Sigma_i \Sigma_k (l_{ik})^2 = 2 \Sigma_i f_i \cdot \Sigma_k f_k x_k^2$$

$\Sigma_i f_i$ is the total number of electrons, n, in the particle, and the length R_1 is defined such that:

$$\Sigma_k f_k \cdot R_1^2 = n R_1^2 = \Sigma_k f_k x_k^2$$

Since f_k is approximately proportional to the mass of the atom,

$$\Sigma m_k \cdot R_1^2 = M R_1^2 = \Sigma m_k x_k^2$$

where M is the total mass of the particle and MR_1^2 the moment of inertia of the particle with respect to the plane normal to OD and passing through the center of gravity. The double summation is then written:

$$\Sigma_i \Sigma_k f_i f_k (l_{ik})^2 = 2 n^2 R_1^2$$

and

$$I/I_e = n^2 \left[1 - h^2 R_1^2 + \cdots \right]$$

where

$$h = \frac{2\pi}{\lambda} \epsilon$$

This is the expansion of the exponential series e^x. Thus the formula for the scattering of an isolated particle is:

$$I/I_e = n^2 e^{-h^2 R_1^2} = n^2 e^{-\frac{4\pi^2}{\lambda^2} R_1^2 \epsilon^2}$$

which is formula (3-3) in Chapter III.

2. Random oriented particles - For randomly oriented and irregularly placed particles, the total intensity is the sum of the intensities diffracted by the individual particles. When there are N particles:

$$I/I_e = n^2 N \left[1 - h^2 \frac{\Sigma^N R_1^2}{N} + \cdots \right]$$

where $\frac{\Sigma_1^N R_1^2}{N}$ represents the mean of the squares of the values of R_1. The mean value of the moment of inertia of a particle in relation to planes of random orientation passing through its center of gravity must be found. From classical mechanics:

$$MR_1^2 = \alpha^2 (MR_x^2) + \beta^2 (MR_y^2) + \gamma^2 (MR_z^2)$$

where MR_x^2 etc. are the moments of inertia with respect to the three principle planes and α, β, γ the direction cosines to the normal of the plane considered. The mean value of R_1^2 is:

$$MR_1^2 = \frac{1}{3} M (R_x^2 + R_y^2 + R_z^2) = \frac{1}{3} MR^2$$

MR^2 being the moment of inertia in relation to the center of gravity, R is the radius of gyration. Therefore:

$$I/I_e = n^2 N \left[1 - \frac{h^2 R^2}{3} + \cdots \right]$$

which is the series expansion of

$$I/I_e = n^2 N e^{-\frac{h^2 R^2}{3}} = n^2 N e^{-\frac{4\pi^2}{3\lambda^2} R^2 \epsilon^2}$$

This is formula(3-4) of Chapter III.